SCIENTIFIC REPORTS

OPEN

SUBJECT AREAS:
TWO-DIMENSIONAL MATERIALS
TRANSMISSION ELECTRON MICROSCOPY
CHARACTERIZATION AND ANALYTICAL TECHNIQUES

Received
22 April 2013

Accepted
10 September 2013

Published
30 September 2013

Correspondence and requests for materials should be addressed to M.O. (ohwada.megumi@nims.go.jp) or K.K. (kimoto.koji@nims.go.jp)

Atomic structure of titania nanosheet with vacancies

Megumi Ohwada[1,2], Koji Kimoto[1], Teruyasu Mizoguchi[3], Yasuo Ebina[4] & Takayoshi Sasaki[4]

[1]Surface Physics and Structure Unit, National Institute for Materials Science, Tsukuba, Ibaraki 305-0044, Japan, [2]Department of Applied Chemistry, Kyushu University, Tsukuba, Ibaraki 305-0044, Japan, [3]Institute of Industrial Science, The University of Tokyo, Meguro, Tokyo 153-8505, Japan, [4]International Center for Materials Nanoarchitectonics, National Institute for Materials Science, Tsukuba, Ibaraki 305-0044, Japan.

Titania nanosheets are two-dimensional single crystallites of titanium oxide with a thickness of one titanium or two oxygen atoms, and they show attractive material properties, such as photocatalytic reactions. Since a titania ($Ti_{0.87}O_2$) nanosheet is synthesized by the delamination of a parent layered $K_{0.8}Ti_{1.73}Li_{0.27}O_4$ crystal using a soft chemical procedure, substantial Ti vacancies are expected to be included and affect the material properties. The atomic arrangement of a titania nanosheet with vacancies has not been revealed owing to the difficulties of direct observation. Here, we have directly visualized the atomic arrangement and Ti vacancies of a titania nanosheet using advanced lower-voltage transmission electron microscopy (TEM). Analyses of the results of first-principles calculations and TEM image simulations for various Ti vacancy structure models indicate that two particular oxygen atoms around each Ti vacancy are desorbed, suggesting the sites where atomic reduction first occurs.

Titania nanosheets[1] are attracting considerable interest owing to their characteristic structures with high crystallinity and ultralow thickness and useful applications as photocatalysts[2], semiconductors[3,4], and dielectric materials[5]. One such titania nanosheet is $Ti_{0.87}O_2$, which is synthesized from a lepidocrocite-type parent material of $K_{0.8}Ti_{1.73}Li_{0.27}O_4$[6]. The crystal structure of titania nanosheets obtained from lepidocrocite-type titanates has been investigated using X-ray diffraction[7], X-ray absorption fine structure[8], and electron diffraction[9]. These studies indicated that the titania nanosheets retain almost the same atomic arrangement of TiO_2 layers as that in the parent materials. This means that titania nanosheets with the composition of $Ti_{0.87}O_2$ include vacancies at Li-substituted Ti sites. In general, atomic vacancies affect the stability of structures and material properties; therefore, it is informative to reveal the atomic structure around Ti vacancies and their distribution in titania nanosheets.

Although transmission electron microscopy (TEM) has high spatial resolution, the observation of atomically thin materials requires not only high spatial resolution but also high sensitivity and low irradiation damage. Electron irradiation damage caused by knock-on effect can be reduced by using lower-voltage TEM at an acceleration voltage below the atomic displacement threshold energies (e.g., approximately 80 kV for carbon and BN nanotubes)[10], and the attainable spatial resolution can be improved by introducing a spherical aberration corrector and a monochromator. Recently, lower-voltage TEM has been frequently applied to the direct observation of atomic defects in graphene[11–13] and related materials (e.g., carbon nanotubes[14,15] and BN nanosheets[16,17]). On the other hand, there have been few observations of oxide nanosheets[18,19], including our previous study, because of the critical irradiation damage during TEM observations. In addition to knock-on damage, transition metal oxides are easily reduced by electron stimulated desorption (ESD)[20,21]. We found that oxide nanosheets are substantially beam-sensitive even at a lower acceleration voltage (e.g., 60 kV), in contrast to the observation of graphene and related materials. Thus, the atomic arrangements of oxide nanosheets have not been visualized at the atomic level.

Here, we report the direct observation of a titania ($Ti_{0.87}O_2$) nanosheet with atomic vacancies. In our previous study, a $Ti_{0.87}O_2$ nanosheet was transformed to a Ti_2O_3 nanosheet through reduction during TEM observation[19]. In the present study, we performed low-voltage and low-dose monochromated TEM without the reduction of the specimen, and we visualized the inherent crystal structure of the titania nanosheet with Ti vacancies. In addition, we introduced first-principles calculations to determine the Ti vacancy structure.

Results

TEM observation of a titania nanosheet. Figure 1 shows (a) a high-resolution TEM image of a titania nanosheet taken in the [010] direction, along with its (b) Fourier transform (i.e., diffractogram) and (c) crystal structure. An

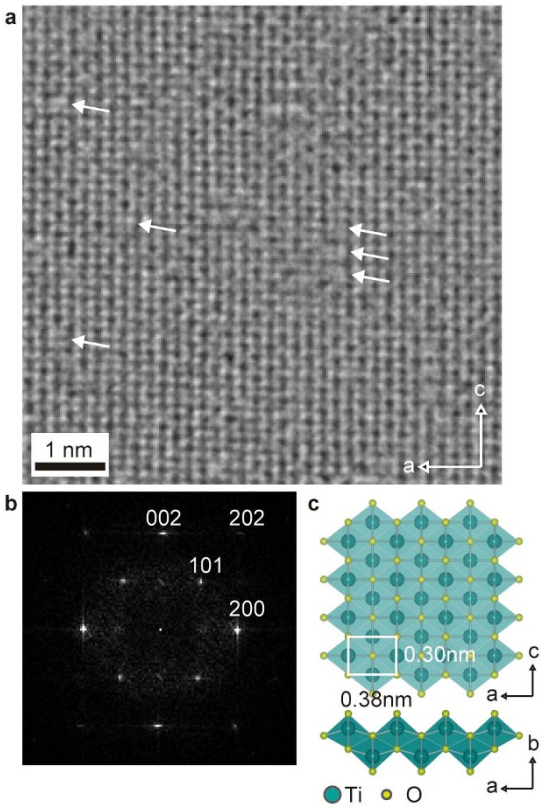

Figure 1 | High-resolution TEM observation of a titania nanosheet. High-resolution TEM image of a titania nanosheet (a) and corresponding Fourier transform (b). Basic structure models of the titania nanosheet in the [010] (upper) and [001] (lower) directions are shown in (c), in which Ti vacancies are not included. The white rectangle in the structure model indicates a unit cell of the titania nanosheet.

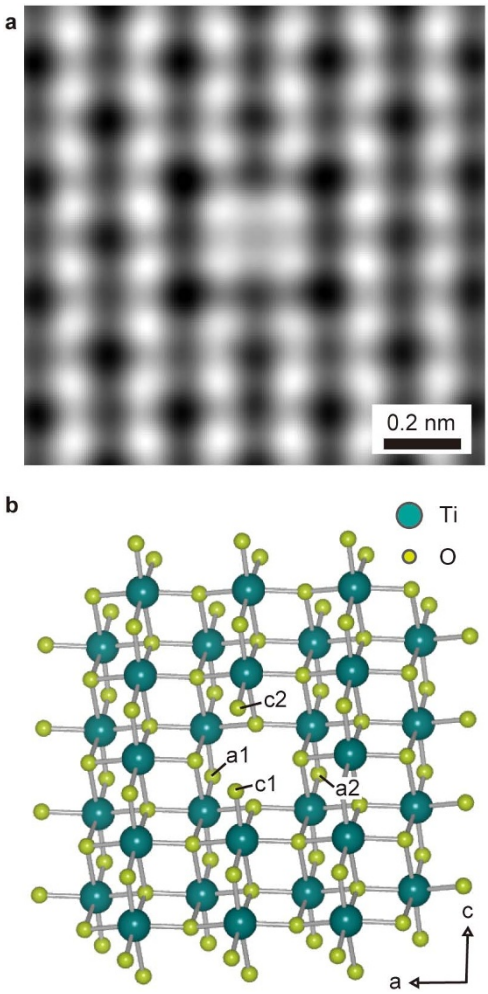

Figure 2 | Atomic structure around a Ti vacancy in the titania nanosheet. (a) Experimental TEM image taken in the [010] direction. Twenty-eight TEM images of bright rectangular areas were summed into one image. (b) Ball and stick model of the titania nanosheet in which one titanium atom at the center is removed. The two oxygen atoms labeled c1 and c2 are coordinated to a single Ti atom, and those labeled a1 and a2 are coordinated to two Ti atoms.

image taken over a relatively wide area is given in Supplementary Fig. S2. As shown in the following TEM image simulation, dark dots correspond to titanium atoms and relatively weak dots correspond to oxygen atoms. Several bright rectangular areas were observed as indicated by arrows, and they are supposed to be atomic vacancies. To clarify the atomic structure of the bright rectangular areas, we summed 28 small portions of TEM images of these areas from the original image shown in Supplementary Fig. S2 (see also Fig. S4). We then obtained an averaged TEM image of the bright areas with a high SN ratio (Fig. 2a).

Structural analyses of Ti vacancies in a titania nanosheet. To investigate the crystal structure of the bright rectangular areas, we compared the experimental TEM image with simulation images obtained using various crystal structure models, in which the atomic arrangements are optimized using first-principles plane-wave basis pseudopotential method. Further details of the first-principles calculations are given in section 3 in Supplementary Information. Figure 3a–c shows three optimized structures and their TEM simulation images, in which the atomic arrangements near the Ti vacancies are different. It is found that the structure optimization is indispensable because it considerably affects each structure and its TEM simulation image. The structures and their TEM simulation images before optimization are given in Supplementary Fig. S8. Figure 3a shows one optimized structure in which a titanium atom is simply removed. In this structure model, some oxygen atoms around the Ti vacancy move slightly outward by about 15 pm from their original positions. The simulation image of this model indicates that the positions of the bright rectangular areas in the experimental image correspond to the vacancies of titanium atoms. The Ti vacancy in the simulation image in Fig. 3a, however, does not precisely reproduce the experimental result. Quantitative analyses of the image intensities are given in Fig. 3d,e, and the intensity of this model along the *a*-axis (Fig. 3d) does not agree with the experimental intensity.

Next, we investigate other Ti vacancy structure models with missing adjacent oxygen atoms. As shown in Fig. 2b, the oxygen atoms around a Ti vacancy are coordinated in various ways, i.e., (i) oxygen atoms c1 and c2 coordinated to a single Ti atom, (ii) oxygen atoms a1 and a2 coordinated to two Ti atoms, and (iii) the others coordinated to three Ti atoms. Figure 3b shows the simulation result for the optimized structure model in which the oxygen atoms c1 and c2 are removed (i,e., Ti + O_{c1} + O_{c2} vacancy model). Figure 3c shows the result for the model in which the other two oxygen atoms a1 and a2 are removed (i.e., Ti + O_{a1} + O_{a2} vacancy model). The atomic arrangements in these optimized structures are differently relaxed through the optimization. In the optimized Ti + O_{c1} + O_{c2} vacancy model, oxygen atoms and the outer titanium atoms on both sides of the Ti vacancy moved outward by 15 and 35 pm, respectively (see the arrows in the structure drawing in Fig. 3b). The simulation image of the Ti + O_{c1} + O_{c2} vacancy model well reproduces the experimental

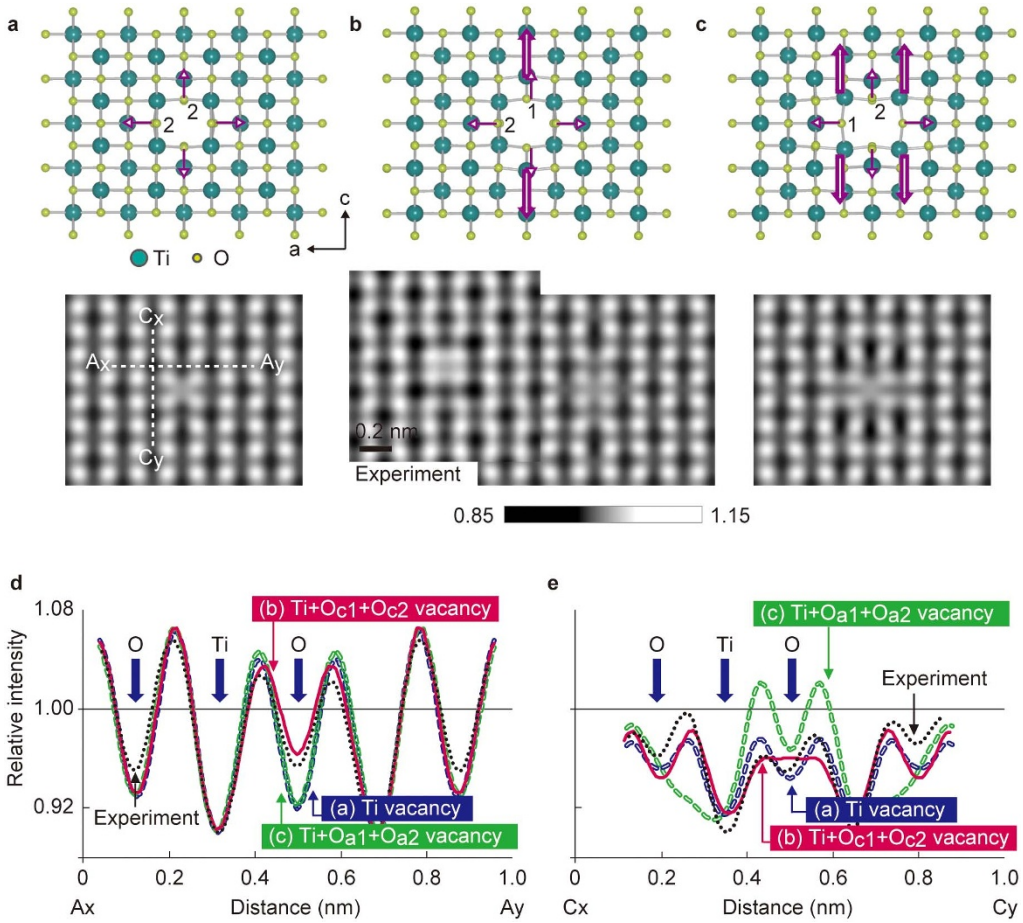

Figure 3 | Simulation results of three types of Ti vacancy structure models and the comparison with experimental result. (a–c) Optimized structures of three Ti vacancy models and their TEM simulation images: (a) simple Ti vacancy model, (b) Ti + O_{c1} + O_{c2} vacancy model, in which one titanium atom and two oxygen atoms (c1 and c2 in Fig. 2b) are removed. The experimental TEM image of Fig. 2a is placed to the left of the simulation image in (b), (c) Ti + O_{a1} + O_{a2} vacancy model, in which one titanium atom and two oxygen atoms (a1 and a2 in Fig. 2b) are removed. The numbers in the structure drawings indicate those of existing oxygen atoms. The arrows in the structure drawings of (a–c) indicate the main directions of atomic distortion during structure optimization by first-principles calculation (large and small arrows indicate titanium and oxygen atoms, respectively). The greyscale bar below the simulation image (b) applies to the three simulation images (a–c). (d,e) Line profiles along the *a*-axis (d) and *c*-axis (e) at the sides of Ti vacancies in the experimental and simulation images. All the simulation profiles are equally scaled to fit the experimental profiles based on the contrast of Ti atoms. Black dotted lines indicate the experimental intensities. Colored lines indicate intensities in the simulation images: Ti vacancy model (a) shown by blue broken lines, Ti + O_{c1} + O_{c2} vacancy model (b) shown by pink solid lines, and Ti + O_{a1} + O_{a2} vacancy model (c) shown by green broken lines.

result, as shown in Fig. 3b. By contrast, the Ti + O_{a1} + O_{a2} vacancy model results in a different configuration of the atoms, for example, the adjacent Ti atoms shift by about 45 pm, and its simulation TEM image has a different appearance, as shown in Fig. 3c.

We elucidate the intensity profiles of the experimental and simulation TEM images, particularly those for the oxygen sites adjacent to Ti vacancies. Figure 3d,e shows the relative intensity profiles along the *a*- and *c*-axes, respectively. TEM image contrast generally depends on atomic potential; therefore, heavy atoms and/or large numbers of atoms exhibit intense dark contrast under the present conditions (a very thin specimen and underfocus imaging). We could estimate the number of oxygen atoms around a Ti vacancy by comparing the contrast of the experimental image with those of simulation images. Note that we can calibrate the intensity by comparing the titanium atomic sites in the experimental and simulation images. The intensity profiles of the simulation images indicated that the Ti + O_{c1} + O_{c2} vacancy model is close to the experimental result in terms of its intensity profiles along the *a*- and *c*-axes (Fig. 3d,e). In other words, the two oxygen atoms c1 and c2 tend to be removed from Ti vacancies. The stability of the structure can also be discussed on the basis of the total energy calculation of each structure model; the results indicate that the Ti + O_{c1} + O_{c2} vacancy model is more stable than the Ti + O_{a1} + O_{a2} vacancy model (see also section 3 in Supplementary Information). In the titania nanosheets, oxygen atoms around Ti vacancies are coordinated to fewer Ti atoms than other atoms and are expected to be easily reconstructed and relaxed to ensure structure stability. Missing oxygen atoms coordinated to fewer Ti atoms have also been discussed in the surface terminations and reduction of bulk TiO_2[22]. In case of the titania nanosheet, single-bonded oxygen atoms around Ti vacancies (O_{c1} and O_{c2}) are considered to be first desorbed in the reduction process to ensure structure stability.

In our previous study[19], we observed a structural phase transformation from $Ti_{0.87}O_2$ nanosheets to Ti_2O_3 nanosheets owing to topotactic-like reduction by electron irradiation. The transformation could be monitored by observing 100 lattice fringes in TEM images. As shown in Fig. 1, the present result of TEM observation does not show such periodicity; therefore, a substantial structural change did not occur during the present observation. The previous experimental results also indicate that the preparation procedure of the TEM specimen does not affect its crystal structure. It is, however, still considered that the oxygen atoms c1 and c2 tend to be removed by the

very weak electron irradiation. Note that such oxygen desorption is difficult to detect using other methods (e.g., electron diffraction) and that direct TEM observation is indispensable for the structure characterization of the vacancies.

Distribution of Ti vacancies in a titania nanosheet. We next observe the distribution of Ti vacancies in the titania nanosheet. Although most of the Ti vacancies are scattered, several types of continuous vacancies can be seen as shown in Fig. 4a–e. The number of these cluster-like Ti vacancies is much smaller than that of single vacancies such as that shown in Fig. 2a, for example, four Ti di-vacancies along the *a*-axis (Fig. 4a) were found in the original image shown in Supplementary Fig. S2. The distribution of Ti vacancies may arise from that of Li^+ ions in the parent $K_{0.8}Ti_{1.73}Li_{0.27}O_4$ layered titanate. In titania nanosheets with the composition of $Ti_{0.87}O_2$, Ti vacancies are considered to be included in an approximate ratio of 13.5%. We can confirm 60 Ti vacancies in Fig. 1a, whose Ti vacancy ratio is calculated to be 7.5% (see also Supplementary Fig. S4). It should be noted that a vacancy ratio of 13.5% is a speculative value based on the mean contents of the parent material and that our present report is the first direct observation of the Ti vacancies in a titania nanosheet.

Discussion

Consequently, we have successfully observed the atomic structure of Ti vacancies in a titania nanosheet using advanced TEM and by first-principles calculations. Lower-voltage TEM with a spherical aberration corrector, a monochromator, and a low-dose technique allows the direct observation of the atomic arrangement around Ti vacancies. In addition, the results of our experiment and analyses by first-principles calculations and TEM image simulations suggest that two particular oxygen atoms around Ti vacancies tend to be removed. This result may be a key to revealing the mechanism and atomic process in the reduction of various titania materials or the fatigue mechanism of titania photocatalysts on their surface.

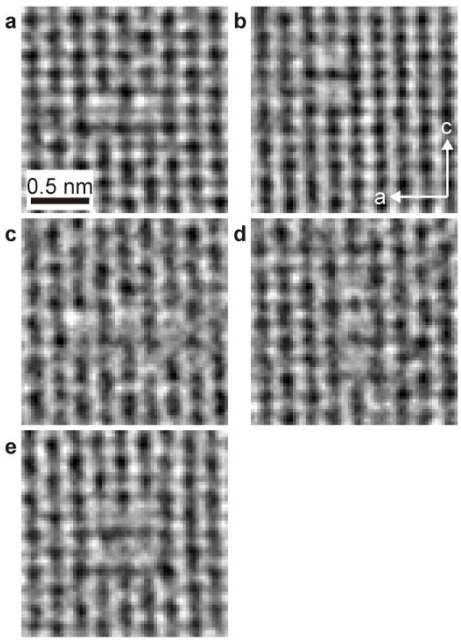

Figure 4 | Various types of cluster-like Ti vacancies in the titania nanosheet. (a) Ti di-vacancy along the *a*-axis (four images were summed). (b) Ti di-vacancy along the *c*-axis (four images were summed). (c) Ti tri-vacancy along the *a*-axis (two images were summed). (d) Ti tri-vacancy along the *c*-axis (one image). (e) 2 × 2 Ti vacancy (three images were summed).

Methods

Preparation of the TEM specimen. A titania ($Ti_{0.87}O_2$) nanosheet was derived by delamination of a $K_{0.8}Ti_{1.73}Li_{0.27}O_4$ layered titanate through a soft chemical procedure[1,23]. In this procedure, K^+ and Li^+ ions in the layered titanate were extracted, and negatively charged $Ti_{0.87}O_2$ layers were formed as colloidal sheets surrounded by tetrabutylammonium ions ($(C_4H_9)_4N^+$). The colloidal suspension of the nanosheets was mounted onto a holey carbon film on a TEM grid. The TEM grid was illuminated with ultraviolet (UV) light in air to photocatalytically decompose the tetrabutylammonium ions surrounding the nanosheets. This self-cleaning treatment by UV light illumination is a standard procedure used in the application of photocatalysts[24]. Further details of the self-cleaning treatment are described in section 1 in Supplementary Information.

TEM experiments. To achieve high-resolution and high-sensitivity observation, we used a transmission electron microscope (FEI, Titan-Cubed) equipped with a spherical aberration corrector and a monochromator. The acceleration voltage of the microscope was set to 80 kV to decrease knock-on damage. We also applied a low dose rate of 2.5×10^4 electrons/nm^2/s and a beam blanking system to reduce the total dose. To improve the contrast and resolution of the TEM images, the energy spread of the incident probe was reduced to 0.1 eV in full width at half maximum using the monochromator. TEM images were recorded by a charge-coupled device (CCD) camera. The defocus of the objective lens was set at an underfocus of about 4 nm. Ten TEM images were acquired each with an exposure time of 2 s, the specimen drift between the TEM images was then corrected, and finally we obtained an image with a high signal-to-noise (SN) ratio by summation of the ten images. Further details of the TEM observation are given in section 2 in Supplementary Information.

TEM image simulation. The TEM image simulation was performed using a multislice simulation program (HREM Research Inc., xHREM). We examined the TEM imaging parameters and selected a third-order spherical aberration coefficient $C_3 = 0$ mm, a defocus spread $\Delta = 2$ nm, and a defocus $z = 4$ nm of underfocus at an acceleration voltage of 80 kV (see also section 2 in Supplementary Information). The effect of the transmission cross coefficient was included in the simulation. Since the experimental TEM image contrast is reduced due to various factors such as modulation transfer function of the CCD camera, the simulated TEM contrast in Fig. 3d,e is reduced to 67% to fit the experimental results.

1. Sasaki, T., Watanabe, M., Hashizume, H., Yamada, H. & Nakazawa, H. Macromolecule-like aspects for a colloidal suspension of an exfoliated titanate. Pairwise association of nanosheets and dynamic reassembling process initiated from it. *J. Am. Chem. Soc.* **118**, 8329–8335 (1996).
2. Shibata, T., Sakai, N., Fukuda, K., Ebina, Y. & Sasaki, T. Photocatalytic properties of titania nanostructured films fabricated from titania nanosheets. *Phys. Chem. Chem. Phys.* **9**, 2413–2420 (2007).
3. Sasaki, T. & Watanabe, M. Semiconductor nanosheet crystallites of quasi-TiO_2 and their optical properties. *J. Phys. Chem. B* **101**, 10159–10161 (1997).
4. Sakai, N., Ebina, Y., Takada, K. & Sasaki, T. Electronic band structure of titania semiconductor nanosheets revealed by electrochemical and photoelectrochemical studies. *J. Am. Chem. Soc.* **126**, 5851–5858 (2004).
5. Osada, M. *et al.* High-*k* dielectric nanofilms fabricated from titania nanosheets. *Adv. Mater.* **18**, 1023–1027 (2006).
6. Sasaki, T. *et al.* A mixed alkali metal titanate with the lepidocrocite-like layered structure. Preparation, crystal structure, protonic form, and acid-base intercalation properties. *Chem. Mater.* **10**, 4123–4128 (1998).
7. Tanaka, T., Ebina, Y., Takada, K., Kurashima, K. & Sasaki, T. Oversized titania nanosheet crystallites derived from flux-grown layered titanate single crystals. *Chem. Mater.* **15**, 3564–3568 (2003).
8. Fukuda, K. *et al.* Nanoarchitecture of semiconductor titania nanosheets revealed by polarization dependent total reflection fluorescence X-ray absorption fine structure. *J. Phys. Chem. B* **108**, 13088–13092 (2004).
9. Sasaki, T., Ebina, Y., Kitami, Y., Watanabe, M. & Oikawa, T. Two-dimensional diffraction of molecular nanosheet crystallites of titanium oxide. *J. Phys. Chem. B* **105**, 6116–6121 (2001).
10. Zobelli, C., Gloter, A., Ewels, C. P., Seifert, G. & Colliex, C. Electron knock-on cross section of carbon and boron nitride nanotubes. *Phys. Rev. B* **75**, 245402 (2007).
11. Meyer, J. C. *et al.* Direct imaging of lattice atoms and topological defects in graphene membranes. *Nano Lett.* **8**, 3582–3586 (2008).
12. Girit, Ç. Ö. *et al.* Graphene at the edge: stability and dynamics. *Science* **323**, 1705–1708 (2009).
13. Warner, J. H. *et al.* Dislocation-driven deformations in graphene. *Science* **337**, 209–212 (2012).
14. Hashimoto, A., Suenaga, K., Gloter, A., Urita, K. & Iijima, S. Direct evidence for atomic defects in graphene layers. *Nature* **430**, 870–873 (2004).
15. Suenaga, K. *et al.* Imaging active topological defects in carbon nanotubes. *Nature Nanotech.* **2**, 358–360 (2007).
16. Alem, N. *et al.* Vacancy growth and migration dynamics in atomically thin hexagonal boron nitride under electron beam irradiation. *Phys. Status Solidi RRL* **5**, 295–297 (2011).
17. Suenaga, K., Kobayashi, H. & Koshino, M. Core-level spectroscopy of point defects in single layer *h*-BN. *Phys. Rev. Lett.* **108**, 075501 (2012).

18. Wang, Y. *et al.* Oxygen vacancy induced structural variations of exfoliated monolayer MnO_2 sheets. *Phys. Rev. B* **81**, 081401 (2010).
19. Ohwada, M. *et al.* Synthesis and atomic characterization of a Ti_2O_3 nanosheet. *J. Phys. Chem. Lett.* **2**, 1820–1823 (2011).
20. Smith, D. J. & McCartney, M. R. The electron-beam-induced reduction of transition metal oxide surfaces to metallic lower oxides. *Ultramicroscopy* **23**, 299–304 (1987).
21. Egerton, R. F. & Malac, M. Radiation damage in TEM and SEM. *Micron* **35**, 399–409 (2004).
22. Diebold, U. The surface science of titanium dioxide. *Surf. Sci. Rep.* **48**, 53–229 (2003).
23. Sasaki, T. & Watanabe, M. Osmotic swelling to exfoliation. Exceptionally high degrees of hydration of a layered titanate. *J. Am. Chem. Soc.* **120**, 4682–4689 (1998).
24. Sasaki, T. *et al.* Titania nanostructured films derived from a titania nanosheet/polycation multilayer assembly via heat treatment and UV irradiation. *Chem. Mater.* **14**, 3524–3530 (2002).

Acknowledgments

We thank K. Suenaga and Y. Sato for useful discussions on the use of lower-voltage electron microscopy. We also thank S. Tominaka for the discussion on titania crystal structures and T. Aizawa for the useful comments on the reduction of transition metal oxides. This work was partially supported by the JST Research Acceleration Program. We used the VESTA program to draw the crystal structures.

Author contributions

TEM measurements were done by K.K. and M.O. T.S. and Y.E. contributed to the synthesis of the materials and discussion of the results. T.M. contributed to first-principles calculations. M.O. and K.K. analyzed the data and wrote the paper with contributions from all authors.

Additional information

Supplementary information accompanies this paper at http://www.nature.com/scientificreports

Competing financial interests: The authors declare no competing financial interests.

How to cite this article: Ohwada, M., Kimoto, K., Mizoguchi, T., Ebina, Y. & Sasaki, T. Atomic structure of titania nanosheet with vacancies. *Sci. Rep.* **3**, 2801; DOI:10.1038/srep02801 (2013).

This work is licensed under a Creative Commons Attribution-NonCommercial-NoDerivs 3.0 Unported license. To view a copy of this license, visit http://creativecommons.org/licenses/by-nc-nd/3.0